

# EES Catalysis

Accepted Manuscript

This article can be cited before page numbers have been issued, to do this please use: W. Zhang, D. Adhikari, S. Ma, Z. Lu, S. Li and T. Alshahrani, *EES Catal.*, 2025, DOI: 10.1039/D5EY00084J.



This is an Accepted Manuscript, which has been through the Royal Society of Chemistry peer review process and has been accepted for publication.

Accepted Manuscripts are published online shortly after acceptance, before technical editing, formatting and proof reading. Using this free service, authors can make their results available to the community, in citable form, before we publish the edited article. We will replace this Accepted Manuscript with the edited and formatted Advance Article as soon as it is available.

You can find more information about Accepted Manuscripts in the [Information for Authors](#).

Please note that technical editing may introduce minor changes to the text and/or graphics, which may alter content. The journal's standard [Terms & Conditions](#) and the [Ethical guidelines](#) still apply. In no event shall the Royal Society of Chemistry be held responsible for any errors or omissions in this Accepted Manuscript or any consequences arising from the use of any information it contains.

## Broader context statement

Solar energy, a clean and abundant resource for synthesizing chemicals, has become a major objective in green chemistry. One issue that has plagued the practical applications of many efficient catalytic systems is their low stability and single cycle use in homogeneous or heterogeneous systems. Therefore, designing efficient, inexpensive, recyclable heterogeneous metal-free photocatalysts will promote environmentally cleaner methods for synthesizing valuable materials. In this work, we contribute a general and effective approach for exploring highly efficient heterogeneous photocatalysts *by constructing photoactive donor-acceptor (D-A) porous organic polymer*. When the two components are connected into a porous organic polymers, a *photo-catalytically favored three-in-one process* is established, which leads to dramatic improvement of photocatalytic performances.



## ARTICLE

## Three-in-One Approach to Fabricate a Porous Porphyrin-Heptazine Polymer for Highly Efficient Visible Light Photocatalysis

Weijie Zhang<sup>a†</sup>, Zhou Lu<sup>a†</sup>, Dipesh Adhikari<sup>b</sup>, Shan Li<sup>a</sup>, Thamraa AlShahrani<sup>c</sup>, Shengqian Ma<sup>\*a</sup>Received 00th January 20xx,  
Accepted 00th January 20xx

DOI: 10.1039/x0xx00000x

Efficient metal-free heterogeneous photocatalysts, using visible light from the sun, continue to be a design challenge for use in chemical synthesis. Compared to metal-free photocatalysts involving a fundamental redox process, multi-dimensional photocatalytic systems with enhanced performance are limited. In this contribution, we demonstrated a general three-in-one approach to construct a donor-acceptor (D-A)-based porous organic polymer *via* connecting the most applied porphyrin with heptazine into a porous framework structure. Herein, a cooperative excitation process for O<sub>2</sub> activation was established that porous organic polymer can not only generate <sup>1</sup>O<sub>2</sub> under light irradiation *via* triplet state, but also capture O<sub>2</sub> and reduce it to O<sub>2</sub><sup>•−</sup>. This synergistic effect dramatically improved the photocatalytic performances, as exemplified in the context of several important aerobic oxidative transformations, including sulfur mustard simulant degradation, oxidative coupling of primary amine molecules, and oxidative conversion of sulfides. Our work, therefore, paves a new way for the development of highly efficient heterogeneous photocatalysts.

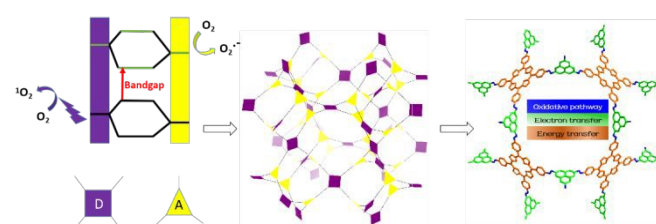
## Introduction

Typically, light-driven oxidative/reductive (redox) processes are limited in semiconductor assemblies, among which electron transfer has been conducted as the primary photo-induced reductive pathway on a single site.<sup>1</sup> In order to incorporate the proper energetics for charge accumulation and separation, some building block molecules, such as porphyrin, perylene, and pyrene, have been employed to combine electron and energy transfer events in supramolecular assemblies.<sup>2</sup> In particular, the advancements of photo-induced electron and energy transfer in a donor-acceptor (D-A) heterojunction facilitate the development of efficient light-harvesting systems.<sup>3,4</sup>

Similarly, the activation of O<sub>2</sub> in an ecological manner occurs by two separate mechanisms: (I) stepwise monovalent reduction *via* an electron-transfer process that O<sub>2</sub> is reduced to O<sub>2</sub><sup>•−</sup>, which can be further disproportionated to form HO<sup>•</sup> and H<sub>2</sub>O<sub>2</sub>, and (II) energy transfer to reverse the spin on one of the unpaired electrons that <sup>1</sup>O<sub>2</sub> is sequentially formed (as shown in Scheme S1). The activation of O<sub>2</sub> is challenging in diverse contexts, ranging from biology to material dissolution. Relatively high oxygen pressure (~5 atm), temperature (~373 K), and/or long-lived N-oxyl radicals such as TEMPO are usually required.<sup>5</sup> As such, we postulate that a three-in-one D-A system photocatalyst designed to include an efficient oxidative pathway,

electron transfer, and energy transfer processes will boost the activation of O<sub>2</sub> in a multi-dimensional photocatalytic system.

Conjugated microporous polymers (CMPs),<sup>6–17</sup> a group of organic porous polymers that combine  $\pi$ -conjugated skeletons with permanent porosity, thermal/chemical stability, high surface area, and structural flexibility, provides a great platform for discovering and designing efficient photocatalysts. CMPs are particularly appealing as they are fine-tunable at the molecular level, allowing for the study of structure-property relationships of the polymers in detail.<sup>18–20</sup> Many studies focused on CMP photocatalysts with favourable energy band positions for stable and efficient organic synthesis.<sup>21–25</sup> Recently, a significant increase in photocatalytic efficiency was achieved by fabricating CMPs through a copolymerization reaction to join donor (D) and acceptor (A) molecules.<sup>26,27</sup>



**Scheme 1.** Schematic Representation of the Donor-Acceptor PHP for proposed three-in-one Photocatalysis.

Bearing the above in mind, we selected two most applied materials in a controlled manner to synergize their properties in the CMP-based D-A system as photocatalysts. Firstly, to improve the light-harvesting abilities of the material, we select porphyrin molecules because they possess a high molar absorptivity and can be custom-designed to target porous materials.<sup>28</sup> Porphyrin molecules have been widely utilized as sensitizers due to their long excited state

<sup>a</sup> Department of Chemistry, University of North Texas, Denton, TX 76203, United States. E-mail: Shengqian.Ma@unt.edu (S. Ma)

<sup>b</sup> Department of Chemical Engineering, University of Virginia, Charlottesville, VA 22903, United States

<sup>c</sup> Department of Physics, College of Science, Princess Nourah bint Abdulrahman University, Riyadh 11564, Saudi Arabia

<sup>†</sup> These two authors contributed equally to this work.

Supplementary Information available: [details of any supplementary information available should be included here]. See DOI: 10.1039/x0xx00000x



lifetimes in energy transfer process.<sup>29–32</sup> In addition, porphyrin dyes are photoactive electron-donors, which benefits in the D-A system.<sup>33</sup> Secondly, graphitic carbon nitride (g-C<sub>3</sub>N<sub>4</sub>), as a metal-free photocatalyst, has been adopted, consisting of heptazine units in layered structure connected at the vertices through amino groups and being demonstrated to be capable of oxidizing amines into imines irradiated by visible light.<sup>34</sup> Structurally, such a robust 3D cage-like ultra-microporous network by [4+3] condensation would result in a high Brunauer-Emmett-Teller (BET) specific surface area as well as good thermal and physicochemical stability. We hypothesize that the combined synergy from heptazine and porphyrin incorporated into the  $\pi$ -conjugated framework will afford an exclusive heterogeneous photocatalytic system benefiting in the aforementioned three-in-one approach (Scheme 1).

## Result and discussion

To demonstrate this proof-of-concept, we started from *meso*-tetra(4-nitrophenyl)porphyrin (TNPP) and heptazine to obtain an azo-linked<sup>35, 36</sup> porous organic polymer in yields up to 63 % (Supporting Information). N<sub>2</sub> sorption isotherms collected at 77 K (Fig. 1a) on the porphyrin-heptazine polymer (PHP) recorded a calculated Brunauer-Emmett-Teller (BET) surface area of ~465 m<sup>2</sup> g<sup>-1</sup> (Langmuir surface area ~707 m<sup>2</sup> g<sup>-1</sup>) and exhibited hysteresis between the adsorption and desorption isotherms. This type of isotherm occurs when a hierarchical porous structure comprising both micropores and mesopores was present as shown in the pore size distribution (Fig. S1). The chemical composition of PHP was further confirmed by solid-state <sup>13</sup>C NMR (Fig. 1b) and <sup>15</sup>N NMR (Fig. S2) spectral analysis.

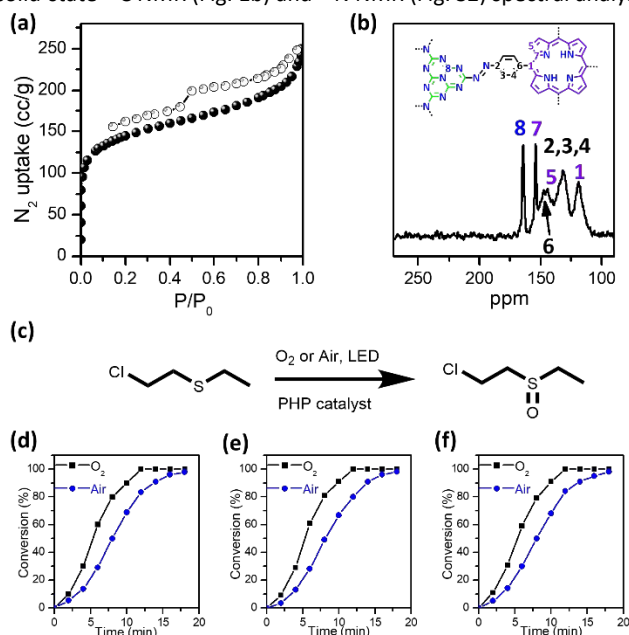


**Fig. 1.** (a) The N<sub>2</sub> adsorption and desorption isotherms of PHP tested at 77 K; (b) Solid-state <sup>13</sup>C CP/MAS NMR spectral of PHP; (c-f) Photooxidation of CEES under LED irradiation and O<sub>2</sub> atmosphere catalyzed by PHP.

Transmission electron microscopy (TEM) images of PHP were interpreted to show that PHP is composed of interconnected porous

nanosheets (Fig. S3). The wider field viewed from scanning electron microscopy (SEM) witnessed a tight network-like structure (Fig. S4). The thermal gravimetric (TG) analysis revealed that PHP has no obvious weight loss, besides adsorbed water, before complete carbonization beginning at 350 °C (Fig. S5). The optical properties of PHP were examined using UV-Vis diffuse reflectance spectroscopy. As shown in Fig. S6, the purple PHP can absorb light over the visible spectrum. Compared to TNPP, PHP is red-shifted by 9 nm, thus confirming bonding between TNPP and heptazine moieties. The absorption band edge of PHP at 687 nm has an optical bandgap value of 1.80 eV.

Reducing the contamination impact of chemical warfare agents (CWAs) is a vital issue.<sup>37</sup> As one representative of CWAs, sulphur mustard is usually detoxified by the selective oxidation strategy. Thus, it is highly desired to design catalysts that can catalytically degrade the sulphur mustard. In the lab, 2-chloroethyl ethyl sulphide (CEES) is an effective sulphur mustard simulant and will be used for our study. Among most reported cases, either hydrogen peroxide (H<sub>2</sub>O<sub>2</sub>) or tert-butyl hydroperoxide (t-BuOOH) has been employed as an oxidant. However, because of their powerful oxidizing ability, it remains challenging to modulate two oxidation products: 2-chloroethyl ethyl sulfoxide (CEESO, target product) and 2-chloroethyl ethyl sulfone (CEESO<sub>2</sub>, by-product). Prominent among extensive efforts that have been undertaken for the oxidation of sulphides into sulfoxides is the O<sub>2</sub> utilization under mild conditions.<sup>37–39</sup> It is imperative to selectively oxidize CEES into CEESO without the possible CEESO<sub>2</sub> generated, particularly under the mild photo-oxidation method, mainly due to the high toxicity of CEESO<sub>2</sub>.

In this strategy, PHP was employed as a photosensitizer to generate <sup>1</sup>O<sub>2</sub> upon LED irradiation. The CEES oxidation in the presence of PHP under O<sub>2</sub> is illustrated in Figure 1c. To perform the oxidation, PHP (0.5 mol%) was suspended in the solvent and then sealed in a glass tube before purging O<sub>2</sub>. CEES was then introduced, and the reaction mixture was monitored by GC-MS (Fig. S7–S8), <sup>1</sup>H NMR (Fig. S9), and <sup>13</sup>C NMR (Fig. S10). As shown, almost no by-product (CEESO<sub>2</sub>) was evident, with a full conversion after 12 min. Figure 1c–1f established the kinetic aspects of the oxidation reaction, for three consecutive injections of CEES into the same reaction irradiated by LED light. The full conversion of the second and third aliquots demonstrated the reusability of the PHP catalyst. For comparison, at 0 min, <sup>13</sup>C NMR peaks at 43, 34, 26, and 15 ppm showed the presence of the mustard gas simulant CEES (Fig. S10). After 12 min, these peaks disappeared, and new peaks were then observed at 53, 45, 36, and 6 ppm, indicating full transformation of CEES into CEESO. Furthermore, an additional catalyst stability test revealed that the conversion remains 100% for 5 cycles with no obvious activity decay (Fig. S11). This result demonstrated that <sup>1</sup>O<sub>2</sub> can be easily generated by PHP upon irradiation with a commercially available LED source.

Moreover, aromatic sulfoxide compounds play a crucial role as intermediates in organic synthesis or as bioactive compounds in the pharmaceutical industry.<sup>40</sup> To further determine the photocatalytic efficiency of PHP, selective photo-oxidation of aromatic sulphides was conducted under the same conditions using visible-light irradiation and O<sub>2</sub> as an oxidant. As depicted in Table S1, it is demonstrated that PHP can catalyse the conversion of a wide range



of sulphides into sulfoxides with remarkable efficiency and high selectivity.

To gain further insight into the three-in-one mechanism, the oxidative coupling of aromatic amines has been selected as the model reaction to investigate the oxidative pathway, electron transfer, and energy transfer processes. This reaction has an essential role in the design and construction of highly valuable building blocks for pharmaceutical applications.<sup>40</sup> However, traditional methods have persistent problems such as poor selectivity, low efficiency, and the requirement of harsh reaction conditions. These prerequisites hamper their widespread applications. A recent report utilized photo-heterogeneous catalysts and O<sub>2</sub> as an oxidant for imine production.<sup>41</sup> In our approach, we also tested PHP as a visible-light photocatalyst for the oxidative coupling reaction of benzylamine (BA) under 1 atm of O<sub>2</sub> at 25 °C. In the absence of light, PHP showed no activity to convert BA into N-benzylidenebenzylamine after three hours (entry 1, Table S2). Similarly, the reaction cannot proceed without PHP irradiated by visible light only (entry 2, Table S2). Control experiments were also carried out for heptazine, TNPP, and g-C<sub>3</sub>N<sub>4</sub> under identical conditions. As shown in Figure S12, after three hours of irradiation, PHP displayed the highest catalytic activity for the benzylamine oxidative coupling (> 99% after 3 h). This compared favourably to the corresponding conversion for free base TNPP (27%), g-C<sub>3</sub>N<sub>4</sub> (13%), and heptazine (10%) (entries 3-5, Table S2). This dramatic enhancement in the catalytic performance of PHP is ascribed to the synergistic effect of heptazine moieties and porphyrin units, which are interconnected throughout the highly porous framework structure. The supernatant after filtration did not afford any other oxidation products, confirming the heterogeneous and robust nature of the PHP catalyst (Fig. S13). Upon completion of the reaction, the simple filtration led to nearly quantitative recovery of PHP without a significant drop in its reactivity (Fig. S14). Importantly, all the photocatalytic reactions tested in this study achieved high selectivity.

High conversion and excellent selectivity were observed when various amine molecules were screened using PHP to assess the electronic effect on the coupling reactions (entries 9-13, Table S2). These outstanding results can presumably be attributed to the high density of accessible active sites in the hierarchical porous structure of PHP, which facilitates the mass transport, thereby assisting high yields in a relatively short period of time. It must be noted that a physical mixture of porphyrin and heptazine showed almost no activity enhancement, suggesting that the covalent interaction of porphyrin with heptazine is necessary.

To gain insights into the above coupling reactions promoted by PHP, a series of thermodynamic and kinetic studies was performed to understand the underlying mechanisms of the photo-redox processes. For the redox coupling reactions to proceed under visible irradiation, the photocatalyst bandgap is required to be close in energy potential to product formation. To estimate the relative positions of the conduction band (CB) and the valence band (VB) edges, electrochemical Mott-Schottky experiments were carried out (Figure 2a). The positive slope of the plot indicated that PHP is a classical n-type semiconductor. From the x-intercept, the CB minimum was determined to be -0.36 V versus Ag/AgCl at pH ~6.6. This result, together with the bandgap energy, enabled us to determine the VB edge at ~1.44 V (Fig. 2b). The CB edge of PHP was

lower compared with g-C<sub>3</sub>N<sub>4</sub>, with ~0.89 V downshift from -1.25 to -0.36 V. These results demonstrated that the incorporation of photoactive electron-donating porphyrin can greatly reduce the CB level of composite, thereby increasing the photo-reduction capability. Taken together, these findings clearly established that PHP has a suitable band structure with a CB level of high photo-reduction capability and a VB level that efficiently facilitates BA oxidation.

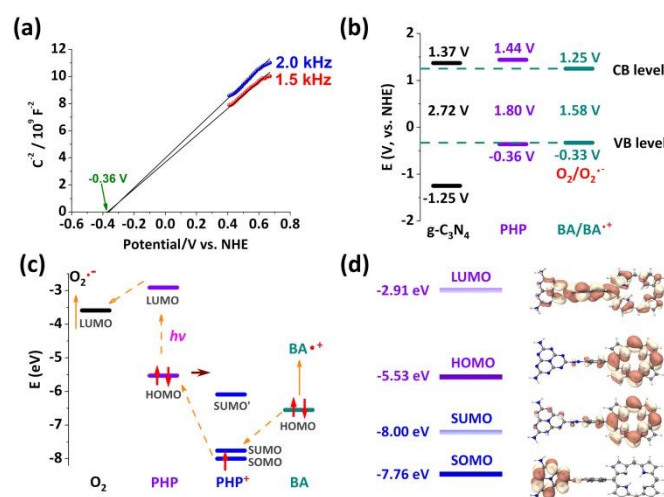


**Fig. 2.** (a) Mott-Schottky plot of sample PHP at 1.5 (red) and 2.0 kHz (blue). (b) Comparison of band gap of g-C<sub>3</sub>N<sub>4</sub><sup>42</sup>, PHP determined in this work, the redox potential of O<sub>2</sub>/O<sub>2</sub><sup>-</sup> (-0.33 eV)<sup>43</sup> and the redox potential of BA/BA<sup>+</sup> (BA= benzylamine)<sup>44</sup>. (c) Calculated energy level diagram and mechanism of fundamental photoredox process. (d) Contours of frontier molecular orbitals of PHP and PHP<sup>+</sup> with isovalues of 0.02 a.u.

To elaborate on the three-in-one mechanism of the photocatalytic reaction and the crucial roles of the photo-generated hole-electron pairs upon oxidative coupling reactions of benzylamines, thermodynamic information about the energy levels were calculated on a porphyrin-heptazine model (Fig. 2c). Since the state of the cationic PHP (PHP<sup>+</sup>, formed during the photocatalytic cycles after electron being transferred to oxygen) is in a doublet spin state, we defined that singly unoccupied molecular orbital (SUMO) and the singly occupied molecular orbital (SOMO) are the lowest unoccupied *beta* orbital and the highest occupied *beta* orbital, respectively. The energy level of LUMO of PHP was higher than that of oxygen, thus leading to catalytically active oxygen radical species O<sub>2</sub><sup>-</sup> (superoxide anion). The HOMO energy level of BA was higher than the SOMO of the PHP<sup>+</sup> (Fig. 2c). Therefore, holes can provide a sufficient thermodynamic driving force to oxidize the BA. Given these findings, it can be concluded that the photo-redox pathway for the oxidative coupling of BA by PHP is completely achievable and most likely to follow an oxidative quenching process as illustrated in Scheme S2.<sup>43</sup>

Next, we investigated the photoluminescence (PL) response to confirm photo-induced hole transfer from PHP to BA (Fig. S15-S16). PL quenching after bubbling O<sub>2</sub> occurred due to the triplet-triplet annihilation (TTA) with photoexcited <sup>3</sup>PHP\* (Fig. S16). This reductive quenching of the PHP could cause the oxidation of BA to yield a BA radical cation, as previously reported.<sup>43</sup> Accordingly, the PHP





exhibited considerably enhanced constant photocurrent, which was almost three times greater than that of pristine g-C<sub>3</sub>N<sub>4</sub>, indicating that more electrons can be photo-generated and then transferred (Fig. S17). It is assumed that the incorporation of porphyrin renders the composite with an increased capacity for light adsorption, and the presence of heptazine facilitates the hole-electron separation and transportation during the photocatalytic process, which is direct evidence to support the proposed mechanism as shown in Scheme S2.

PL emission quenching is in line with catalysts displaying a higher photocatalytic activity.<sup>45</sup> Notably, the steady-state PL measurement (Fig. S18) displayed a significant PL emission quenching, suggesting a greatly suppressed radiative hole-electron recombination in PHP compared to TNPP. To elucidate the kinetics of the trap state, time-resolved PL technique was conducted to find the emission lifetimes of  $12.07 \pm 0.03$  and  $5.94 \pm 0.03$  ns for TNPP and PHP at 712 nm (Fig. 3a), respectively. The shorter PL lifetime arises from rapid charge transfer between the donor (porphyrin) and acceptor (heptazine) units, which quenches exciton emission in favor of generating long-lived charges. Therefore, the enhanced photocurrent and quenched PL together result in enhanced photocatalytic performance for the PHP material.<sup>45</sup>

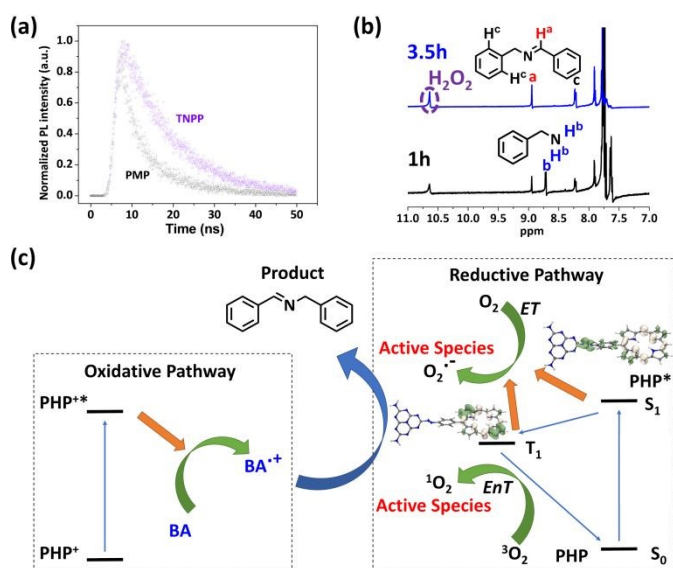


**Fig. 3.** (a) Time-resolved PL kinetics for TNPP (purple point) and PHP (black point), recorded with excitation at 420 nm and emission at 712 nm. (b) <sup>1</sup>H NMR spectra of the reaction mixture after 1 hour (black) and 3.5 hours (blue), showing the formation of H<sub>2</sub>O<sub>2</sub> and imine product. (c) Proposed three-in-one reaction mechanism combining oxidative and reductive pathways. Inset figures are electron density difference (EDD) maps of corresponding excited states of PHP with isovalue of 0.0005 a.u. BA: benzylamine; ET: electron transfer; EnT: energy transfer.

Superoxide radicals have been previously reported to abstract one hydrogen atom at the benzylic position of the BA radical cation, thereby forming benzylimine and the by-product hydrogen peroxide in a 1:1 ratio.<sup>46</sup> Therefore, the reaction mixture of BA coupling was monitored by <sup>1</sup>H NMR spectroscopy to observe the formation of H<sub>2</sub>O<sub>2</sub>

at 10.95 ppm (Fig. 3b and Fig. S19). The integrated peak areas between H<sub>2</sub>O<sub>2</sub> and benzenemethanamine were found with a ratio of 1:1.4. From this result, we concluded that the oxidative coupling reaction follows both expected energy transfer and electron transfer pathways, whereas the latter one was the predominant mechanism.

To kinetically monitor electron transfer from BA to O<sub>2</sub> promoted by PHP, 1,4-bis(dimethylamino)benzene was used as an indicator molecule to track the superoxide radical (O<sub>2</sub><sup>•-</sup>) formation.<sup>45</sup> The electron transfer from the 1,4-bis(dimethylamino)benzene to dioxygen gave rise to the formation of a cationic radical complex in blue colour (Fig. S20). As shown in Fig. S21, the photocatalytic properties associated with the generation of singlet oxygen (<sup>1</sup>O<sub>2</sub>) upon irradiation of PHP were explored using 1,3-diphenylisobenzofuran (DPBF).<sup>47</sup> Through the electron density difference (EDD) map of PHP at T<sub>1</sub> state, the TNPP unit mainly contributed to the electron excitation (Fig. 3c). However, time-dependent absorbance decay of DPBF revealed a fast consumption upon <sup>1</sup>O<sub>2</sub> in the presence of PHP, while a slower decay was observed in the presence of TNPP only, suggesting the lower photoactivity (Fig. S22). This result highlighted that the incorporation of the porphyrin and heptazine moieties promoted the reactivity.

Similar results were observed in spin trap electron paramagnetic resonance (EPR) experimental results using 2,2,6,6-tetramethylpiperidinyloxy (TEMPO) and 5,5-dimethyl-1-pyrroline N-oxide (DMPO) as <sup>1</sup>O<sub>2</sub> and O<sub>2</sub><sup>•-</sup> trapping agents, respectively. As shown in Fig. S23 and S24, both catalytically active oxygen radical species O<sub>2</sub><sup>•-</sup> and <sup>1</sup>O<sub>2</sub> were evidenced in EPR results. A greater EPR intensity was observed by PHP comparing to TNPP only, validating that PHP can generate more <sup>1</sup>O<sub>2</sub> via energy transfer. To sum, the EPR results confirmed the coexistence of both reaction pathways of electron transfer (to produce superoxide anion radical O<sub>2</sub><sup>•-</sup>) and energy transfer (to produce singlet oxygen <sup>1</sup>O<sub>2</sub>) in the oxidative benzylamine coupling reactions.

The rates of the photocatalytic reaction of benzylamines and its para-substituted derivatives (X = OMe, H, Me and Cl groups) have been investigated using PHP and TNPP to obtain the Hammett plot (Fig. S25 and S26). A linear relationship between log(k<sub>x</sub>/k<sub>h</sub>) values and Brown-Okamoto constant (σ<sub>p</sub><sup>+</sup>) parameters<sup>48</sup> was fitted with a downward slope, thereby implying that the hole transfer from porphyrin π-cation radicals in PHP to benzylamine substrate to give a positive-charged intermediate (Fig. 3c). Based on the aforementioned results and the comparison between the cooperative effect of O<sub>2</sub><sup>•-</sup> and <sup>1</sup>O<sub>2</sub> in the reaction over PHP, it is concluded <sup>1</sup>O<sub>2</sub> as the sole ROS source. This behaviour accounts for the poor activity of TNPP as depicted in Table S2, entry 3. Moreover, the fact that there is no clear linearity correlation between log(k<sub>x</sub>/k<sub>h</sub>) and σ<sub>p</sub><sup>+</sup> in the Hammett plot (Fig. S26), attests for the lack of positive-charged intermediates which are generated by hole activation pathway by TNPP catalysts.

Control experiments suggested that only trace product was observed in the absence of either light or PHP as a photocatalyst, respectively (entries 2 and 3, Table S3). Thus, to discern the assignments and the reaction mechanism of the photogenerated electron/hole pairs in the photochemical transformation of benzylamine to imine, further control experiments were undertaken. Practically, upon replacing O<sub>2</sub> with N<sub>2</sub> gas, we found that benzylamine was hardly transformed to the corresponding product



(entry 4, Table S3). This observation emphasizes the important role of oxygen in the reaction. However, the addition of potassium iodide (KI), as the hole scavenger, resulted in a lower conversion of 29 % (entry 5, Table S3). When adopting sodium azide as the singlet oxygen  $^1\text{O}_2$  scavenger, a conversion of 64% was obtained (entry 6, Table S3). The addition of P-benzoquinone (BQ), as  $\text{O}_2^{\cdot-}$  scavenger, under the same conditions, resulted in a low yield of the desired product (entry 7, Table S3).

Based on these findings, it was concluded that the following three-in-one mechanisms are responsible for the remarkable photocatalytic activity of PHP (Fig. 3c). For the reductive pathway, photo-induced electrons in the CB level of PHP are strong reductants that are capable of capturing  $\text{O}_2$  onto the surface and accordingly reduce it to  $\text{O}_2^{\cdot-}$ . Meanwhile, the  $\text{PHP}^+$  is generated during the photocatalytic cycles after the electron being transferred to oxygen. Spontaneously, the photo-generated holes on the  $\text{PHP}^+$  oxidize the substrate BA to yield the benzylamine cation radical ( $\text{BA}^{\cdot+}$ ). The porphyrin units in PHP can generate  $^1\text{O}_2$  species under light irradiation via the triplet state. For the oxidative pathway, the  $\text{BA}^{\cdot+}$  can be oxidized by both activated oxygen species, separately. Here,  $\text{O}_2^{\cdot-}$  radical first produces a highly reactive  $\text{HO}_2^{\cdot}$  species that later oxidizes the  $\text{BA}^{\cdot+}$  to the product.  $^1\text{O}_2$  subsequently oxidizes the  $\text{BA}^{\cdot+}$  to the product directly.

Taken together, the combined experimental and theoretical results support the preferred active sites in PHP for oxidative coupling reactions and the electron transfer pathway at the porphyrin and heptazine moieties, respectively. The incorporation of porphyrin molecules into the  $\pi$ -conjugated framework allows the separation of the reduction and oxidation sites as well as the modification of the electronic density of porphyrin. Such a cooperative activation process benefits not only the energy transfer pathway but also the spatial charge separation, thus improving the photocatalytic process involved in the simultaneous reactions.

## Conclusions

In summary, we report a novel porous porphyrin-heptazine polymer as designed three-in-one photocatalyst for organic transformations. As evidenced by the mechanistic insight into thermodynamics and kinetics, the high photocatalytic efficiency reflects the synergistic effects on the electron transfer pathway (superoxide anion radical) and the energy transfer pathway (singlet oxygen). Furthermore, we demonstrated that the basic mechanism in this study is universal, and similar principles can be applied to create other porous organic polymer catalysts through three-in-one approach. It is thus believed that these findings potentially provide new avenues towards more energy-efficient photocatalysts and related energy conversion systems.

## Conflicts of interest

There are no conflicts to declare.

## Acknowledgements

The authors acknowledge the Robert A. Welch Foundation (B-0027) for financial support of this work. Partial support from Princess Nourah bint Abdulrahman University Researchers Supporting Project number (PNURSP2025R1), Princess Nourah bint Abdulrahman University, Riyadh, Saudi Arabia (T.A.) is also acknowledged.

## Notes and references

1. A. Hagfeldt and M. Graetzel, *Chem Rev*, 2002, **95**, 49-68.
2. M. Gilbert and B. Albinsson, *Chem Soc Rev*, 2015, **44**, 845-862.
3. P. Heremans, D. Cheyns and B. P. Rand, *Acc Chem Res*, 2009, **42**, 1740-1747.
4. R. C. Coffin, J. Peet, J. Rogers and G. C. Bazan, *Nat Chem*, 2009, **1**, 657-661.
5. R. Neumann and M. Dahan, *Nature*, 1997, **388**, 353-355.
6. J.-S. M. Lee and A. I. Cooper, *Chem Rev*, 2020, **120**, 2171-2214.
7. X. Gao, C. Shu, C. Zhang, W. Ma, S.-B. Ren, F. Wang, Y. Chen, J. H. Zeng and J.-X. Jiang, *J Mater Chem A*, 2020, **8**, 2404-2411.
8. K. Zhang, W. Liu, Y. Gao, X. Wang, Z. Chen, R. Ning, W. Yu, R. Li, L. Li, X. Li, K. Yuan, L. Ma, N. Li, C. Shen, W. Huang, K. Xie and K. P. Loh, *Adv Mater*, 2021, **33**, e2006323.
9. F. Lan, Q. Wang, H. Chen, Y. Chen, Y. Zhang, B. Huang, H. Liu, J. Liu and R. Li, *ACS Catal*, 2020, **10**, 12976-12986.
10. L. Stegbauer, S. Zech, G. Savasci, T. Banerjee, F. Podjaski, K. Schwinghammer, C. Ochsenfeld and B. V. Lotsch, *Adv Energy Mater*, 2018, **8**, 1703278.
11. J. Wu, F. Xu, S. Li, P. Ma, X. Zhang, Q. Liu, R. Fu and D. Wu, *Adv Mater*, 2019, **31**, 1802922.
12. S. Lee, G. Barin, C. M. Ackerman, A. Muchenditsi, J. Xu, J. A. Reimer, S. Lutsenko, J. R. Long and C. J. Chang, *J Am Chem Soc*, 2016, **138**, 7603-7609.
13. Q. Sun, Z. Dai, X. Meng and F. S. Xiao, *Chem Soc Rev*, 2015, **44**, 6018-6034.
14. Z. Xiang, R. Mercado, J. M. Huck, H. Wang, Z. Guo, W. Wang, D. Cao, M. Haranczyk and B. Smit, *J Am Chem Soc*, 2015, **137**, 13301-13307.
15. Y. Xu, S. Jin, H. Xu, A. Nagai and D. Jiang, *Chem Soc Rev*, 2013, **42**, 8012-8031.
16. Y. Xie, T. T. Wang, X. H. Liu, K. Zou and W. Q. Deng, *Nat Commun*, 2013, **4**, 1960.
17. Y. L. Zhu, H. Long and W. Zhang, *Chem Mater*, 2013, **25**, 1630-1635.
18. G. Zhang, Z.-A. Lan and X. Wang, *Angew Chem Int Ed*, 2016, **55**, 15712-15727.
19. R. S. Sprick, J. X. Jiang, B. Bonillo, S. Ren, T. Ratvijitvech, P. Guiglion, M. A. Zwiijnenburg, D. J. Adams and A. I. Cooper, *J Am Chem Soc*, 2015, **137**, 3265-3270.
20. J. Chun, S. Kang, N. Park, E. J. Park, X. Jin, K. D. Kim, H. O. Seo, S. M. Lee, H. J. Kim, W. H. Kwon, Y. K. Park, J. M. Kim, Y. D. Kim and S. U. Son, *J Am Chem Soc*, 2014, **136**, 6786-6789.
21. Z. A. Lan, G. Zhang, X. Chen, Y. Zhang, K. A. I. Zhang and X. Wang, *Angew Chem Int Ed*, 2019, **131**, 10342-10346.
22. Z. Mi, T. Zhou, W. Weng, J. Unruangsri, K. Hu, W. Yang, C. Wang, K. A. I. Zhang and J. Guo, *Angew Chem Int Ed*, 2021, **60**, 9642-9649.
23. W. Huang, N. Huber, S. Jiang, K. Landfester and K. A. I. Zhang, *Angew Chem Int Ed*, 2020, **59**, 18368-18373.
24. X. Wang, L. Chen, S. Y. Chong, M. A. Little, Y. Wu, W. H. Zhu, R. Clowes, Y. Yan, M. A. Zwiijnenburg, R. S. Sprick and A. I. Cooper, *Nat Chem*, 2018, **10**, 1180-1189.



25. L. Wang, Y. Wan, Y. Ding, S. Wu, Y. Zhang, X. Zhang, G. Zhang, Y. Xiong, X. Wu, J. Yang and H. Xu, *Adv Mater*, 2017, **29**, 1702428.
26. Y. Xu, N. Mao, C. Zhang, X. Wang, J. Zeng, Y. Chen, F. Wang and J.-X. Jiang, *Appl Catal B: Environ*, 2018, **228**, 1-9.
27. L. Li, Z. Cai, Q. Wu, W. Y. Lo, N. Zhang, L. X. Chen and L. Yu, *J Am Chem Soc*, 2016, **138**, 7681-7686.
28. H. J. Son, S. Jin, S. Patwardhan, S. J. Wezenberg, N. C. Jeong, M. So, C. E. Wilmer, A. A. Sarjeant, G. C. Schatz, R. Q. Snurr, O. K. Farha, G. P. Wiederrecht and J. T. Hupp, *J Am Chem Soc*, 2013, **135**, 862-869.
29. X. Chen, M. Addicoat, E. Jin, L. Zhai, H. Xu, N. Huang, Z. Guo, L. Liu, S. Irle and D. Jiang, *J Am Chem Soc*, 2015, **137**, 3241-3247.
30. S. U. Raut, K. R. Balinge, S. A. Deshmukh, S. H. Barange, B. C. Mataghare and P. R. Bhagat, *Catal Sci Tech*, 2022, **12**, 5917-5931.
31. S. U. Raut, S. A. Deshmukh, S. H. Barange and P. R. Bhagat, *Catal Today*, 2023, **408**, 81-91.
32. S. U. Raut and P. R. Bhagat, *Fuel*, 2021, **303**.
33. S. Jin, M. Supur, M. Addicoat, K. Furukawa, L. Chen, T. Nakamura, S. Fukuzumi, S. Irle and D. Jiang, *J Am Chem Soc*, 2015, **137**, 7817-7827.
34. F. Su, S. C. Mathew, L. Mohlmann, M. Antonietti, X. Wang and S. Blechert, *Angew Chem Int Ed*, 2011, **50**, 657-660.
35. P. Arab, M. G. Rabbani, A. K. Sekizkardes, T. Islamoglu and H. M. El-Kaderi, *Chem Mater*, 2014, **26**, 1385-1392.
36. H. A. Patel, S. H. Je, J. Park, D. P. Chen, Y. Jung, C. T. Yavuz and A. Coskun, *Nat Commun*, 2013, **4**, 1357.
37. A. Atilgan, M. M. Cetin, J. Yu, Y. Beldjoudi, J. Liu, C. L. Stern, F. M. Cetin, T. Islamoglu, O. K. Farha, P. Deria, J. F. Stoddart and J. T. Hupp, *J Am Chem Soc*, 2020, **142**, 18554-18564.
38. M. Cao, R. Pang, Q. Y. Wang, Z. Han, Z. Y. Wang, X. Y. Dong, S. F. Li, S. Q. Zang and T. C. W. Mak, *J Am Chem Soc*, 2019, **141**, 14505-14509.
39. Y. Liu, S. Y. Moon, J. T. Hupp and O. K. Farha, *ACS Nano*, 2015, **9**, 12358-12364.
40. I. Fernandez and N. Khiar, *Chem Rev*, 2003, **103**, 3651-3705.
41. B. Chen, L. Wang and S. Gao, *ACS Catal*, 2015, **5**, 5851-5876.
42. Z. J. Wang, S. Ghasimi, K. Landfester and K. A. Zhang, *Chem Commun*, 2014, **50**, 8177-8180.
43. P. M. Wood, *Biochem J*, 1988, **253**, 287-289.
44. Z. J. Wang, S. Ghasimi, K. Landfester and K. A. Zhang, *Adv Mater*, 2015, **27**, 6265-6270.
45. H. Q. Xu, J. Hu, D. Wang, Z. Li, Q. Zhang, Y. Luo, S. H. Yu and H. L. Jiang, *J Am Chem Soc*, 2015, **137**, 13440-13443.
46. J. H. Park, K. C. Ko, E. Kim, N. Park, J. H. Ko, D. H. Ryu, T. K. Ahn, J. Y. Lee and S. U. Son, *Org Lett*, 2012, **14**, 5502-5505.
47. J. Park, D. Feng, S. Yuan and H. C. Zhou, *Angew Chem Int Ed*, 2015, **54**, 430-435.
48. C. Xu, H. Liu, D. Li, J. H. Su and H. L. Jiang, *Chem Sci*, 2018, **9**, 3152-3158.

View Article Online  
DOI: 10.1039/D5EY00084J





### Data Availability Statement

The data that support the findings of this study are available from the corresponding author upon reasonable request. This includes raw and processed data generated during the current study. Any additional data or materials required for replication of the results can also be provided by the corresponding author.

